JACS
JOURNAL OF THE AMERICAN CHEMICAL SOCIETY

Article

pubs.acs.org/JACS

Porphodilactones as Synthetic Chlorophylls: Relative Orientation of β-Substituents on a Pyrrolic Ring Tunes NIR Absorption

Xian-Sheng Ke,[†] Yi Chang,[‡] Jia-Zhen Chen,[†] Jiangwei Tian,[‡] John Mack,[§] Xin Cheng,[†] Zhen Shen,*[,‡] and Jun-Long Zhang*[,†,‡]

[†]Beijing National Laboratory for Molecular Sciences, State Key Laboratory of Rare Earth Materials Chemistry and Applications, College of Chemistry and Molecular Engineering, Peking University, Beijing 100871, P.R. China

[‡]State Key Laboratory of Coordination Chemistry, School of Chemistry and Chemical Engineering, Nanjing University, Nanjing 210093 P.R. China

[§]Department of Chemistry, Rhodes University, Grahamstown 6140, South Africa

Supporting Information

ABSTRACT: Porphodilactones represent the porphyrin analogues, in which the peripheral bonds of two pyrrole rings are replaced by lactone moieties. They provide an opportunity to investigate how β-substituent orientation of porphyrinoids modulates the electronic structures and optical properties, in a manner similar to what is observed with naturally occurring chlorophylls. In this work, a comprehensive description of the synthesis, characterization, and optical properties of *meso*-tetrakispentafluorophenylporphodilactone isomers is first reported. The β-dilactone moieties are found to lie at opposite pyrrole positions (*trans*- and *cis*-configurations are defined by the relative orientations of the carbonyl group when one lactone moiety is fixed), in accordance with earlier computational predictions (Gouterman, M. *J. Am. Chem. Soc.* **1989**, *111*, 3702). The relative orientation of the β-dilactone moieties has a significant influence on the electronic structures and photophysical properties. For example, the Q_y band of *trans*-porphodilactone is red-shifted by 19 nm relative to that of the *cis*-isomer, and there is a 2-fold increase in the absorption intensity, which resembles the similar trends that have been reported for natural chlorophyll *f* and *d*. An in depth analysis of magnetic circular dichroism spectral data and TD-DFT calculations at the B3LYP/6-31G(d) level of theory demonstrates that the *trans*- and *cis*-orientations of the dilactone moieties have a significant effect on the relative energies of the frontier π-molecular orbitals. Importantly, the biological behaviors of the isomers reveal their different photocytotoxicity in NIR region (>650 nm). The influence of the relative orientation of the β-substituents on the optical properties in this context provides new insights into the electronic structures of porphyrinoids which could prove useful during the development of near-infrared absorbing photosensitizers.

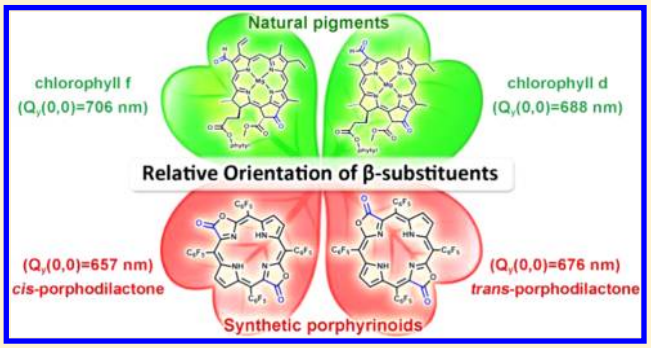

INTRODUCTION

The β-position substituents of naturally occurring tetrapyrrole pigments have been found to play an important role in shaping the optical properties in the near-infrared (NIR) region.[1] In contrast, traditional synthetic approaches for modulating the properties of porphyrin ligands have tended to involve an extension of the π-system or the size of the macrocycle.[2] The successful design of NIR absorbing porphyrinoids, which more closely mimic the properties of naturally occurring tetrapyrroles, would provide new insights into the electronic structures of these molecules, in a manner that should facilitate the development of applications in optical materials and biological studies. The recently discovered chlorophyll *f* ($Q_{y(0,0)}$ = 706 nm)[3] has a formyl group located at the C2 position (Figure 1) and a dramatically red-shifted Q_y band compared to chlorophyll *b* ($Q_{y(0,0)}$ = 648 nm)[1b] and *d* ($Q_{y(0,0)}$ = 688 nm)[1d] which have formyl groups at the C7 and C3 positions, respectively (Figure 1). Although this demonstrates that modulating the orientation of the β-substituents is a viable strategy for fine-tuning the optical properties of natural pigments, the use of a similar approach has yet to emerge in synthetic porphyrin chemistry. Herein, we report the synthesis and characterization of porphodilactones, in which the two peripheral lactone moieties lie at opposite pyrrole positions (shown in Figure 1), and investigate the effect of the relative orientation of the β-dilactone moieties (*trans*- and *cis*-configurations are defined based on the relative orientations of the carbonyl groups) on the electronic structures and optical and biological properties.

Porpholactones, in which at least one pyrrole ring of the porphyrin ligand is replaced by an oxazolone moiety, have attracted increasing attention in recent years.[4] The incorpo-

Received: March 26, 2014

   dx.doi.org/10.1021/ja502729x | J. Am. Chem. Soc. XXXX, XXX, XXX−XXX

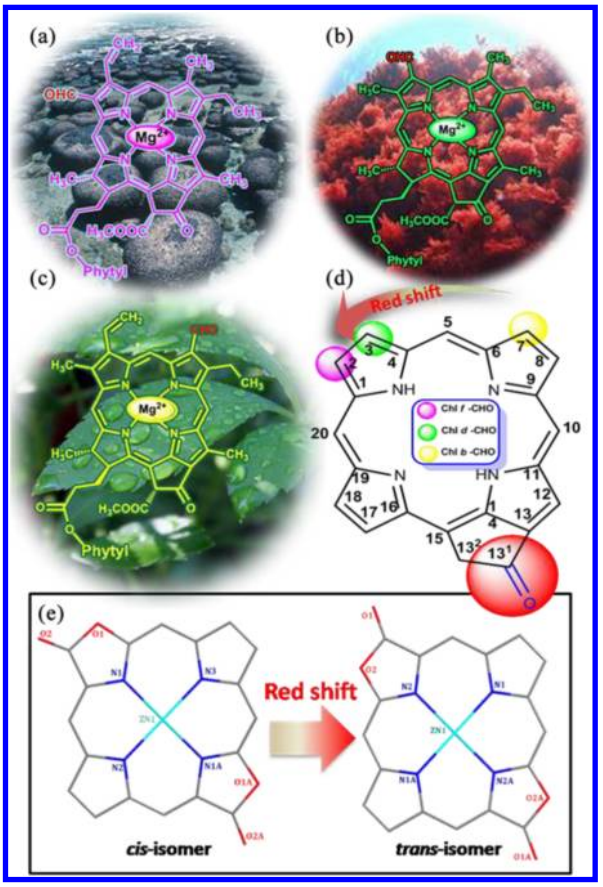

Figure 1. Chemical structures (a) Chl *f*, (b) *d*, (c) *b* and (d) the orientation of *β*-formyl groups (purple: Chl *f*; green: Chl *d*; yellow: Chl *b*); (e) stick models of the single crystal X-ray structures of *cis*-Zn(py$_2$)F$_{20}$TPPDL and *trans*-Zn(py$_2$)F$_{20}$TPPDL, axial pyrindines, *meso*-phenyl group, and protons omitted for clarity.).

ration of the oxazolone group results in optical properties that lie between those of porphyrins and chlorins,[4b,d] due to their lower molecular symmetry and the partial saturation of the porphyrin periphery. Porpholactones provide attractive platforms for designing catalysts for atom transfer reactions, novel optical materials, and photodynamic therapy (PDT) photosensitizers.[5] The obvious next step is to explore the properties of porphyrin analogues with two lactone moieties. In a seminal paper on the subject by Gouterman and co-workers,[4b] porphodilactones were tentatively identified, and their structures were assigned using computational calculations as shown in Figure S1. Given the wide range of possible orientations for the dilactone moieties, the definitive characterization of these isomers became a bottleneck hindering further progress, and this has impeded the emergence of a definitive understanding of the relationship between the structures and electronic properties of porphodilactones.

In this work, we found that the *β*-dilactone moieties were located at the opposite pyrrole positions in tetrakispentafluorophenylporphodilactones (H$_2$F$_{20}$TPPDL), which is consistent with Gouterman's earlier assignments based on the prediction that the total energies of these structures are significantly lower than those of the adjacent isomers (>0.84 eV).[4b] The $Q_y(0,0)$ transition of *trans*-porphodilactone is red-shifted by 19 nm compared to that of the *cis*-isomer, and there is a 2-fold increase in the absorption intensity. Similar trends have been reported for natural chlorophyll *f* and *d*, indicating that the relative orientations of the *β*-substituents have a significant effect on the photophysical properties. Magnetic circular dichroism (MCD) spectral data and theoretical calculations have been carried out to analyze the influence of the relative orientation of *β*-dilactone moieties on the relative energies of the frontier *π*-MOs and hence on the optical properties. The photophysical properties of the porphodilactones and their photocytotoxicity toward cancer cells upon excitation at NIR regions (>650 nm) have also been investigated. The insights achieved on this basis should assist the future rational design of NIR region PDT photosensitizers.

RESULTS AND DISCUSSION

Synthesis and Characterization of the Opposite *trans*- and *cis*-Porphodilactones and Their Zinc Complexes. Reactions of tetrakispentafluorophenylporphyrin (H$_2$F$_{20}$TPP) and tetrapentakisfluorophenylporpholatone (H$_2$F$_{20}$TPPL) with an excess of Oxone (H$_2$F$_{20}$TPP: 12 equiv and H$_2$F$_{20}$TPPL: 4 equiv), in the presence of catalytic amounts of RuCl$_3$ and 2,2′-bipyridine, resulted in the formation of porphodilactone isomers (H$_2$F$_{20}$TPPDL, Scheme 1) in 45 and 53% yield,

Scheme 1. Synthetic Procedure for Porphodilactone Isomers[a]

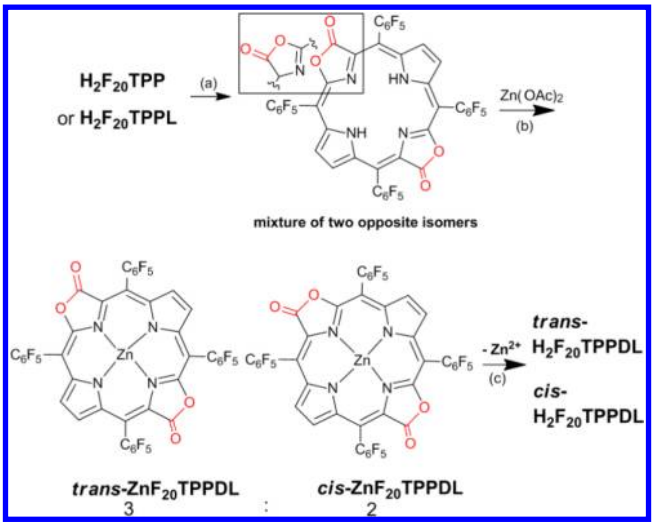

[a](a) 20% RuCl$_3$, 20% 2,2′-bipyridine, 4−12 equiv oxone, H$_2$O/1,2-dichloroethane (1:1), 70 °C; (b) Zn(OAc)$_2$, CHCl$_3$/CH$_3$OH (v/v = 7:3), reflux; (c) HCl solution (36−38%), acetone.

respectively. However, several attempts to separate the porphodilactone isomers using silica gel chromatography, HPLC, TLC, recrystallization, and even supercritical fluid chromatography all failed (Figures S2−5). To isolate the porphodilactone isomers, we metalized the porphodilactone isomers with Zn(OAc)$_2$ so that the *trans*- and *cis*-ZnF$_{20}$TPPDL isomers could be separated by silica gel chromatography (18 and 8% yields, respectively) (Figure S6). Subsequent demetallization of the ZnF$_{20}$TPPDL isomers by HCl solution (36−38%) afforded pure porphodilactone free base isomers in quantitative yield.

The characterization of *trans*- and *cis*-H$_2$F$_{20}$TPPDL and their zinc complexes was carried out by ^{1}H-, ^{13}C- and ^{19}F-NMR and IR spectroscopy and by HR-ESI MS (Figure S19−35). As shown in Figure 2, an analysis of the ^{1}H NMR spectra demonstrates that the mixture of porphodilactones contains

dx.doi.org/10.1021/ja502729x | J. Am. Chem. Soc. XXXX, XXX, XXX−XXX

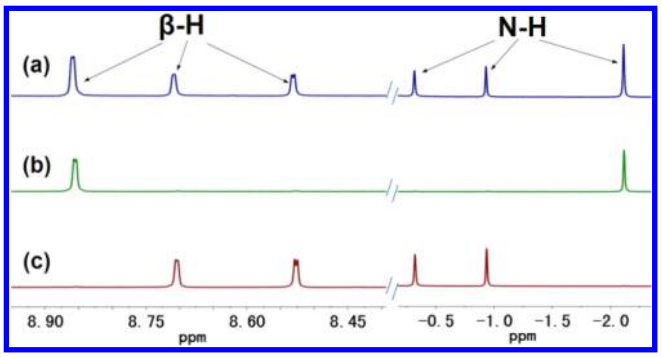

Figure 2. ^{1}H NMR spectra (500 MHz) of mixture (a) the mixture of *trans*- and *cis*-H_2F_{20}TPPDL (blue line), (b) *trans*-H_2F_{20}TPPDL (green line), and (c) *cis*-H_2F_{20}TPPDL (red line) in $CDCl_3$.

only the opposite forms, which have been termed the *trans*- and *cis*-isomers in the context of this study. It should be noted that similar results were obtained by using both Gouterman's and our experimental procedures.[4b,f] In the ^{1}H NMR spectrum of *trans*-H_2F_{20}TPPDL (Figure 2), one proton signal lies at δ = 8.86 (d, J = 1.7 Hz, 4H) (β-H) and another lies at −2.12 (s, 2H) (N−H) ppm. This simple pattern reflects the symmetry of the structure. In contrast, the spectrum of *cis*-H_2F_{20}TPPDL is more complicated with two peaks observed at δ = 8.53(d, J = 2.0 Hz, 2H) and 8.70 (d, J = 1.4 Hz, 2H) (β-H) ppm and another two peaks at δ = −0.32 (s, 1H) and −0.94 (s, 1H) (N−H) ppm, due to the change in the alignment of the main C_2 symmetry axis. The IR spectra (Figure S31−34) also differ based on the orientation of the β-dilactone moieties. C═O vibration bands are observed at 1769 cm^{-1} for *trans*-H_2F_{20}TPPDL and 1771 and 1790 cm^{-1} for *cis*-H_2F_{20}TPPDL. Similar spectral features are observed for *trans*- and *cis*-ZnF_{20}TPPDL.

Recrystallization of ZnF_{20}TPPDL isomers in dichloromethane (DCM) (in the presence of 1% pyridine and benzene) gave single crystals appropriate for X-ray diffraction analysis. The unit cells of both *trans*- (CCDC: 987687) and *cis*-ZnF_{20}TPPDL (CCDC: 987686) contain two independent molecules. The details are provided as Tables S1−2. The X-ray structures in Figure 3 reveal the differing lactone moiety arrangements of *trans*- and *cis*-ZnF_{20}TPPDL. The two lactone rings of *trans*-ZnF_{20}TPPDL are correlated to one another by a C_2 axis perpendicular to the porphyrinoid plane, while the C_2 axis of *cis*-ZnF_{20}TPPDL lies in the plane. The porphyrinoid plane of *trans*-ZnF_{20}TPPDL is much less distorted from planarity than that of *cis*-ZnF_{20}TPPDL (Figure 3c,d). The C═O bond distances are 1.208 and 1.184 Å for *trans*- and *cis*-ZnF_{20}TPPDL, respectively. In each case, the Zn centers are octahedrally coordinated by four pyrrole nitrogen atoms with Zn−N bond distances ranging from 2.019 to 2.053 Å and those of the two axial pyridine ligands with Zn−N bond distances ranging from 2.344 to 2.443 Å. Interestingly, the axial pyridyl N−Zn bonds of *trans*-ZnF_{20}TPPDL (2.344 Å) are shorter than those of *cis*-ZnF_{20}TPPDL (2.443 Å). This might be due to a slight deviation (4.5°) of the axial Zn−N4 (pyridine) bond relative to the normal line of the porphyrinoid plane (N1, N1A, N2, N3, and Zn1) in the case of *cis*-ZnF_{20}TPPDL (Figure 3d). The angle between the two axially coordinated pyridine ligand planes of *cis*-ZnF_{20}TPPDL is 17.6°. In contrast, the two axial pyridines of *trans*-ZnF_{20}TPPDL are coplanar. These results suggest that the relative orientation of the dilactone moieties on

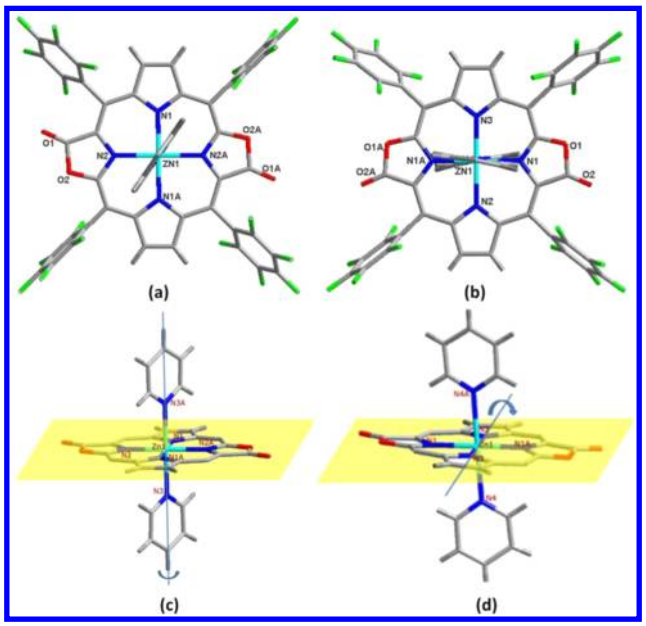

Figure 3. Stick models of the single crystal X-ray structures of (a) *trans*-$Zn(py_2)F_{20}$TPPDL and (b) *cis*-$Zn(py_2)F_{20}$TPPDL. The alignment of the C_2 symmetry axis for (c) *trans*-$Zn(py_2)F_{20}$TPPDL is orthogonal to the porphodilactone π-system and (d) the *cis*-isomer lies in the plane of the porphodilactone π-system.

the β-periphery influences the coordination of the central metal ion.

Optical Spectra of *trans*- and *cis*-H_2F_{20}TPPDLs and Their Zinc Complexes. The electronic absorption spectra were measured in DCM (Figure 4) to investigate the effects of β-dilactone orientation on optical properties. When compared with the spectrum of H_2F_{20}TPPL, *trans*- and *cis*-H_2F_{20}TPPDL have broad B (or Soret) bands centered at 410 and 408 nm, respectively, with pronounced shoulders of intensity to the blue. There is remarked red-shift of the Q bands between 500−700 nm. The most likely explanation for this is that there is strong electronic coupling between the lactone moieties and the main porphyrin chromophores. Interestingly, *trans*-H_2F_{20}TPPDL has a red-shifted (ca. 19 nm when compared to *cis*-isomer) phyllo-type Q-band region in which the ε_{max} value of the lowest energy Q-band is twice that of the *cis*-isomer (Figure 4). This suggests that the relative orientation of the dilactone moieties plays a significant role in determining the energies of the frontier π-MOs. Metalation with zinc(II) leads to red-shifted and largely unresolved B bands (ca. 15 and 17 nm, respectively) and blue-shifted Q_y bands (ca. 13 and 22 nm). This is the pattern normally observed for metalloporphyrinoids upon coordination of the free base compound by Zn(II) ion.[6] It is noteworthy that *trans*-ZnF_{20}TPPDL has a chlorin-type UV−vis absorption spectrum with a very intense Q_y band ($\varepsilon_B/\varepsilon_{Q@663}$= 1.8).

The fluorescence spectra of *trans*- and *cis*-H_2F_{20}TPPDLs and their zinc complexes exhibit well-resolved vibronic progressions upon excitation in the B band region. As shown in Figure 5, each emission spectrum contains one intense dominant band (I_{0-0}) centered in the 644−678 nm region and a shoulder (I_{0-1}) slightly to the red. Small Stokes shifts are observed relative to the lowest energy Q bands, as is characteristic of most porphyrinoids.[6] When compared to the spectrum of H_2F_{20}TPPL, the main emission bands of *trans*- and *cis*-H_2F_{20}TPPDL are red-shifted by ca. 35 and 23 nm, respectively,

dx.doi.org/10.1021/ja502729x | J. Am. Chem. Soc. XXXX, XXX, XXX−XXX

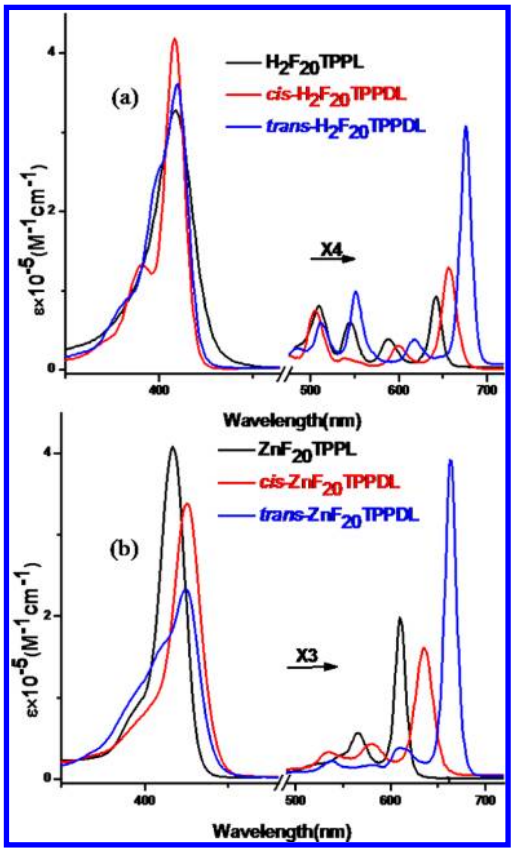

Figure 4. UV−vis absorption spectra of (a) H_2F_{20}TPPL, *trans*- and *cis*-H_2F_{20}TPPDL and (b) ZnF_{20}TPPL, *trans*- and *cis*-ZnF_{20}TPPDL in DCM.

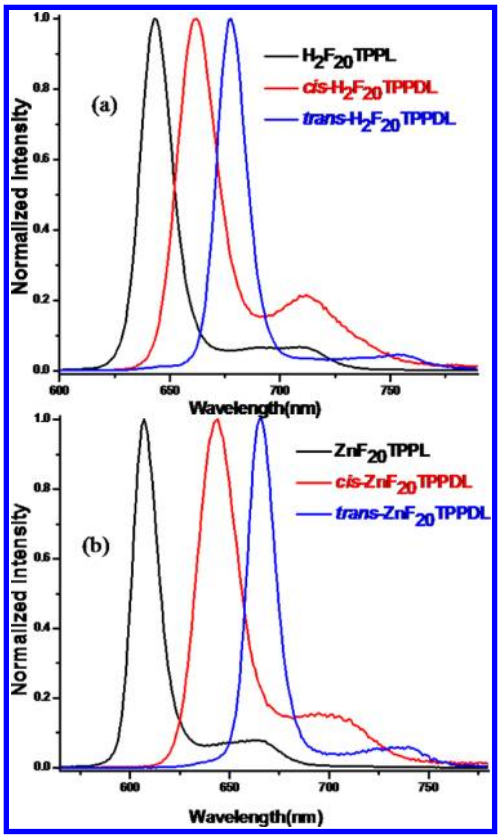

Figure 5. Emission spectra of (a) H_2F_{20}TPPL, *trans*- and *cis*-H_2F_{20}TPPDL (excited at B band region); (b) ZnF_{20}TPPL, *trans*- and *cis*-ZnF_{20}TPPDL (excited at B band region) in DCM.

and the fluorescence quantum yields (Φ_F) are slightly lower (0.10 and 0.09 vs 0.13 for H_2F_{20}TPPL). For the zinc complexes, the fluorescence emission bands are shifted to the blue by 12 and 18 nm compared to those of free bases with a 3- to 4-fold decrease in the Φ_F values (0.025 for *trans*-ZnF_{20}TPPDL and 0.028 for *cis*-ZnF_{20}TPPDL). Shortened lifetimes (from 3.49 to 0.65 ns for *trans*-F_{20}TPPDL, and from 3.49 to 0.81 ns for *cis*-F_{20}TPPDL) are also observed (Table S3). These trends are probably related to an increase in intersystem crossing due to the heavy atom effect. The excitation spectra for the free bases and zinc complexes were identical with the absorption spectra when monitored at their maximum emission bands (I_{0-0}). This demonstrates that the emission originated from the lowest lying $\pi-\pi^*$ transition (Figure S7−10).

The redox potentials for the porphodilactones provide an insight into their electronic structures. Cyclic voltammograms (CV) were measured, and the data are listed in Table 1. Both free base porphodilactone isomers have two quasi-reversible reduction waves at ∼−0.4 and −0.9 V and a quasi-reversible oxidation wave at ∼+1.60 V (Figure S11). The HOMO−LUMO gaps obtained from the first-oxidation and -reduction potentials of *trans*-H_2F_{20}TPPDL (1.98 eV) is narrower than that of *cis*-H_2F_{20}TPPDL (2.10 eV). As would normally be anticipated, the HOMO−LUMO gaps calculated from the electrochemical data are consistent with those obtained from the optical data (1.80 and 1.84 eV). Similar trends are observed in the CV of *trans*-ZnF_{20}TPPDL relative to *cis*-ZnF_{20}TPPDL. Compared to H_2F_{20}TPP, H_2F_{20}TPPL, and their zinc complexes, the experimental and calculated HOMO−LUMO gaps of porphodilactones are consistent to their absorptions. These data reveal that the relative orientations of the lactone moieties play a significant role in shaping the electronic structures and the optical properties in the Q-band region.

Electronic Structures of *trans*- and *cis*-H_2F_{20}TPPDLs and Their Zinc Complexes. A series of MCD measurements were made and B3LYP optimizations and TD-DFT calculations were carried out to analyze the effect of dilactone orientation on the optical properties and electronic structures. MCD spectroscopy is based on intensity mechanisms described by the Faraday $\mathcal{A}_1$, $\mathcal{B}_0$, and $\mathcal{C}_0$ terms.[10] TD-DFT calculations were carried out on a series of B3LYP-optimized geometries using the Coulomb-attenuated B3LYP functional (CAM-B3LYP) functional with 6-31G(d) basis sets, since the results of TD-DFT calculations with the B3LYP functional of the Gaussian 09 software package[11] are known to be problematic when significant charge transfer character is involved.[12] The CAM-B3LYP functional includes a long-range correction of the exchange potential, which incorporates an increasing fraction of Hartree−Fock (HF) exchange as the interelectronic separation increases. Moffitt[13] and Michl[14] demonstrated that the relative intensities of the major electronic absorption bands of aromatic π-systems can be successfully described in terms of perturbations to the structure of a high-symmetry parent hydrocarbon ($C_{16}H_{16}^{2-}$ in the case of metal tetrapyrrole porphyrinoid complexes or $C_{18}H_{18}$ for free base compounds). The nodal patterns of the π-system MOs are retained even when the symmetry of the cyclic perimeter is modified. As a consequence of this, there is an $M_L = 0, \pm 1, \pm 2, \pm 3, \pm 4, \pm 5, \pm 6, \pm 7, 8$ sequence in ascending energy terms in the π-MOs of metal porphyrinoids. Within the band nomenclature of

dx.doi.org/10.1021/ja502729x | J. Am. Chem. Soc. XXXX, XXX, XXX−XXX

Table 1. CV Data (V vs SCE) for $H_2F_{20}TPP$, $H_2F_{20}TPPL$, *trans* and *cis*-$H_2F_{20}TPPDLs$ and Their Zinc Complexes in CH_2Cl_2 Containing 0.1 M NBu_4PF_6

	oxidation		reduction				
compounds	second	first	first	second	third	HOMO–LUMO gap (V)[a]	HOMO–LUMO gap (eV)[b]
trans-$H_2F_{20}TPPDL$		+1.61	−0.37	−0.87		1.98	2.34
cis-$H_2F_{20}TPPDL$		+1.66	−0.44	−0.85		2.10	2.45
trans-$ZnF_{20}TPPDL$	+1.54	+1.25	−0.75	−1.28		2.00	2.24
cis-$ZnF_{20}TPPDL$		+1.31	−0.86	−1.06	−1.28	2.17	2.41
$H_2F_{20}TPP$	+1.77	+1.55	−0.76	−1.17		2.31	2.80
$H_2F_{20}TPPL$		+1.77	−0.58	−1.04		2.35	2.64
$ZnF_{20}TPP$	+1.36	+1.20	−1.05	−1.47		2.25	2.94
$ZnF_{20}TPPL$	+1.57	+1.29	−0.76	−1.20		2.05	2.62

[a]The potential difference between the first oxidation and first reduction. [b]Calculation results with the B3LYP functional.

Gouterman's 4-orbital model,[6] there is an electronically allowed B transition and a forbidden Q transition linking the frontier $M_L = \pm 4, \pm 5$ π-MOs based, respectively, on $\Delta M_L = \pm 1$ and ± 9 transitions. When a structural perturbation results in a marked lifting of the degeneracy of the MOs derived from the HOMO and/or LUMO of the parent perimeter (referred to as the ΔHOMO and ΔLUMO values within Michl's terminology[14]) there is a mixing of the allowed and forbidden properties of the Q and B bands and a marked intensification of the Q-band.[15] When ΔHOMO ≈ ΔLUMO the Q bands remain relatively weak, since the orbital angular momentum properties of the parent hydrocarbon perimeter are retained.[16]

Michl[14] introduced an **a**, **s**, **−a** and **−s** terminology for the four MOs derived from the HOMO and LUMO of the parent perimeter so that π-systems of porphyrinoids with differing molecular symmetry and with different relative orderings of the four frontier π-MOs in energy terms can be readily compared (Figure 6). One MO derived from the HOMO of the parent perimeter and another derived from the LUMO have nodal planes which coincide with the *yz*-plane and are referred to, respectively, as the **a** and **−a** MOs, while the corresponding MOs with antinodes on the *yz*-plane are referred to as the **s** and **−s** MOs. The D_{4h} symmetry of porphyrin ligand dianions dictates that the **−a** and **−s** MOs are degenerate since the $M_L = \pm 5$ nodal patterns differ along the *x*- and *y*-axes only by being rotated by 90° with respect to each other (Figure 6). Both $H_2F_{20}TPP$ and $ZnF_{20}TPP$ are predicted to have very small ΔHOMO and ΔLUMO values (Figure 6). When lactone moieties are introduced to form porpholactones and -dilactones (Figure 7), the **s** and **−a** MOs, which lack significant MO coefficients on these moieties, are predicted to be significantly stabilized in the free base compounds and zinc complexes relative to the corresponding TPP compounds, due to the inductive effects associated with the structural modification. In contrast, there is a smaller stabilization of the **a** and **−s** MOs, which have larger MO coefficients on the lactone moieties, probably due to the mesomeric interaction between the peripheral carbonyl bond and the π-system MOs. The orientation of the carbonyl bonds has a more significant effect on the relative energies of the **−a** and **−s** MOs of the *cis*- and *trans*-dilactone isomers (Figure 7), since the nodal patterns of the MOs derived from the LUMO of the parent perimeter are not radially symmetric. This results in large ΔLUMO values for *trans*-H_2 and *trans*-$ZnF_{20}TPPDL$ (Figures 6 and 7) and accounts for the intensification of the Q bands that is observed in Figure 4, since the ΔLUMO values are significantly greater than the ΔHOMO values (Figure 6).

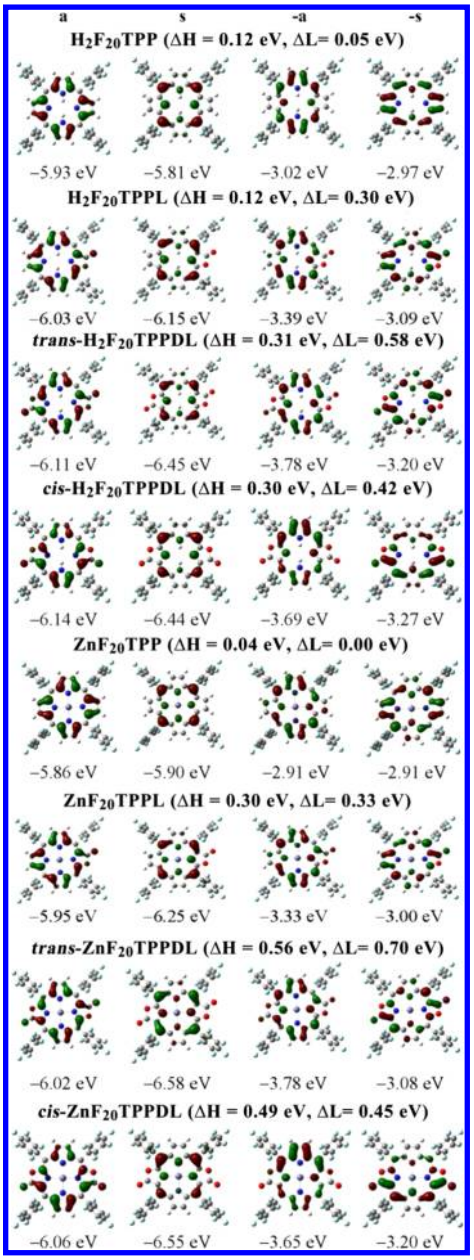

Figure 6. Nodal patterns and energies of the frontier π-MOs of $H_2F_{20}TPP$, $H_2F_{20}TPPL$ and *trans*- and *cis*-$H_2F_{20}TPPDL$ and of $ZnF_{20}TPP$, $ZnF_{20}TPPL$ and *trans*- and *cis*-$ZnF_{20}TPPDL$ in TD-DFT calculations with the B3LYP functional.

dx.doi.org/10.1021/ja502729x | J. Am. Chem. Soc. XXXX, XXX, XXX–XXX

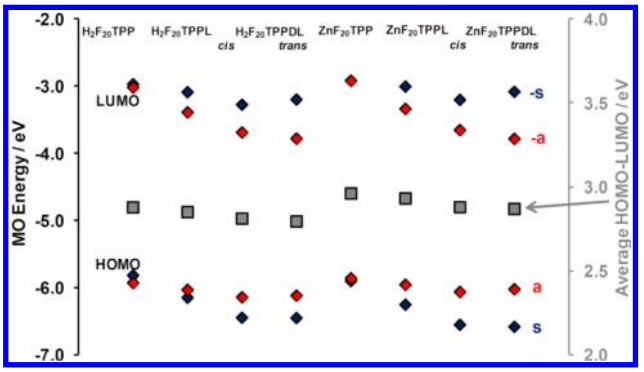

Figure 7. Energies of the **a** and −**a** MOs of $H_2F_{20}TPP$, $H_2F_{20}TPPL$ *cis*- and *trans*-$H_2F_{20}TPPDL$, $ZnF_{20}TPP$, $ZnF_{20}TPPL$, and *cis*- and *trans*-$ZnF_{20}TPPDL$ in the TD-DFT calculations carried out with the B3LYP functional are denoted with red diamonds, while those of the **s** and −**s** MOs are denoted with blue diamonds. Gray squares are used to plot the average HOMO−LUMO gap taking all four MOs of Michl's perimeter model into account against a secondary axis.

The main electronic Q and B bands of the *cis* and *trans* isomers can be readily assigned, since the $\mathcal{A}_1$ terms that would be anticipated in the MCD spectra of metal porphyrin complexes are replaced by coupled pairs of oppositely signed $\mathcal{B}_0$ terms due to the absence of a 3-fold or higher axis of symmetry (Figure 7 and Table S4). Michl[14] has demonstrated that in the context of aromatic π-systems such as porphyrinoids, the differential absorbance of left and right polarized light by the excited states is related to the alignments of the induced magnetic moments with and against the axis of light propagation, and the applied field (and hence the ordering of the MCD signs for the Q_x, Q_y, B_x, B_y bands) is determined primarily by the relative magnitudes of the ΔHOMO and ΔLUMO values. When a structural perturbation introduces a large ΔHOMO or ΔLUMO value, circulation of charge on the perimeter is hindered. The relative magnitudes of the ΔHOMO and ΔLUMO values, therefore, determine whether the circulation of the excited electron in the LUMO level or that of the hole left in the HOMO level is the dominant factor in conserving the quantum of orbital angular momentum provided by the incident photon of left or right circularly polarized light. When ΔHOMO > ΔLUMO and electronic charge circulation in the LUMO predominates, the ordering of the MCD intensity signs for the $\mathcal{B}_0$ terms associated with the Q and B bands is −, +, −, + in ascending energy terms. In contrast, when ΔLUMO > ΔHOMO and the circulation of the positive charge associated with the hole left in the HOMO is the dominant factor, the sequence reverses to +, −, +, −. Djerassi and co-workers[17] demonstrated in the context of chlorin compounds where |ΔHOMO − ΔLUMO| ≈ 0, that the sign sequence of the forbidden Q bands often changes before that of the allowed B bands when ΔHOMO > ΔLUMO, so that a +, −, −, + sign sequence is observed in the MCD spectrum. This is the pattern that is observed for *trans*-H_2 and *trans*-$ZnF_{20}TPPDL$. In contrast, a −, +, −, + sign sequence is observed for both *cis*-H_2 and *cis*-$ZnF_{20}TPPDL$ (Figure 8). Although this would only be anticipated for *cis*-$ZnF_{20}TPPDL$ based on the predicted MO energies (Figure 6), it should be noted that the differences between the predicted ΔHOMO and ΔLUMO values are relatively small in this context and there is more scope for conformational flexibility with the free base compounds. The sign sequences observed in the MCD spectra for the $\mathcal{B}_0$ terms

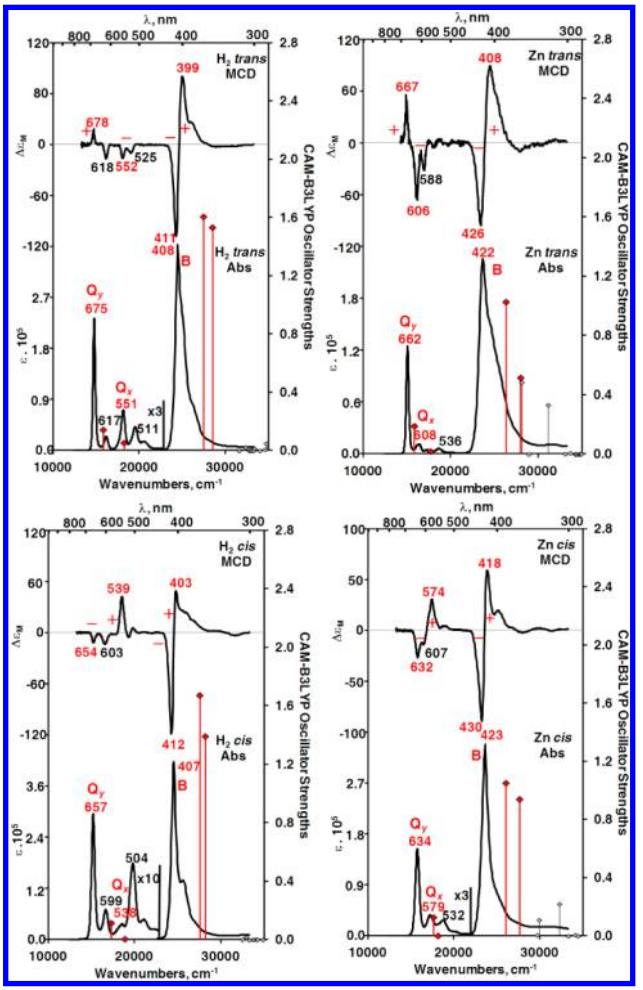

Figure 8. Absorption and MCD spectra of *cis*-$H_2F_{20}TPPDL$ (H_2 *cis*) and *cis*-$ZnF_{20}TPPDL$ (Zn *cis*) (bottom) and of *trans*-$H_2F_{20}TPPDL$ (H_2 *trans*) and *trans*-$ZnF_{20}TPPDL$ (Zn *trans*) (top) in $CHCl_3$. TD-DFT spectra calculated with the CAM-B3LYP functional were plotted against a secondary axis. Large red diamonds and wavelength label are used to highlight the main electronic Q and B bands. The details of the TD-DFT spectra and a comparison of the calculated and observed intensities of the main spectral bands are provided as Table S4.

associated with the Q and B bands are broadly consistent with the trends that would be anticipated based on the MO energies predicted in the B3LYP geometry optimizations and hence help to validate the theoretical descriptions of the electronic structures.

Photosensitizing Properties of the Porphodilactones in the NIR Region. Although the use of porphyrins and their derivatives in PDT is well-known,[7] their major shortcoming in this regard is their relatively weak absorption at the red end of the visible region. Since the absorption intensities of the *trans*- and *cis*-$H_2F_{20}TPPDLs$ and their zinc complexes are 66, 22, 179, and 53 times greater than that of $H_2F_{20}TPP$ when the extinction coefficient ratio of Q(0,0) band and B band ($\varepsilon_{Q(0,0)}/\varepsilon_B$) is taken into consideration, the obvious next step was to investigate their $^1O_2$ photosensitizing properties upon excitation at NIR region.

Singlet oxygen quantum yields (Φ_Δ) of *trans*- and *cis*-$H_2F_{20}TPPDLs$ and their zinc complexes were calculated using 1,3-diphenyl isobenzofuran (DPBF) as a singlet oxygen scavenger.[8] When *trans*-$H_2F_{20}TPPDL$ and its zinc complex were analyzed, mixed solutions of the sensitizer and DPBF were

dx.doi.org/10.1021/ja502729x | J. Am. Chem. Soc. XXXX, XXX, XXX−XXX

Table 2. Singlet Oxygen Quantum Yields (Φ_Δ) of H_2F_{20}TPP, H_2F_{20}TPPL, *trans*- and *cis*-H_2F_{20}TPPDLs and their zinc complexes in DCM

compounds	Φ_Δ[a]
trans-H_2F_{20}TPPDL	0.53[b]
trans-ZnF_{20}TPPDL	0.66[b]
cis-H_2F_{20}TPPDL	<0.05[c]
cis-ZnF_{20}TPPDL	0.87[c]
H_2F_{20}TPP	n.d.[d]
ZnF_{20}TPP	n.d.[d]
H_2F_{20}TPPL	0.84[c]
ZnF_{20}TPPL	n.d.[d]

[a]Methylene blue (MB) as standard (Φ_Δ = 0.57 in DCM). [b]Excited by a 671 nm laser beam. [c]Excited by a 635 nm laser beam. [d]Not determined due to too weak absorption at 635 and 671 nm.

irradiated with a 671 nm laser beam. The slope of the graph obtained by plotting the changes in absorbance of DPBF at 411 nm against irradiation time was used to calculate the Φ_Δ value (Figures S12−18). Values of 0.53 and 0.66 were obtained for *trans*-H_2F_{20}TPPDL and *trans*-ZnF_{20}TPPDL in DCM refers to methylene blue (MB) (Φ_Δ = 0.57 in DCM). Φ_Δ values of *cis*-H_2F_{20}TPPDL and its zinc complex were analyzed by using similar method. A value of 0.87 was obtained for *cis*-ZnF_{20}TPPDL when irradiated with a 635 nm laser beam. As the control experiments, we chose H_2F_{20}TPP, H_2F_{20}TPPL and their zinc derivatives and found that their singlet oxygen quantum yields, except for H_2F_{20}TPPL (0.84), could not be measured due to the extremely low absorption at 635 and 671 nm. To our surprise, *cis*-H_2F_{20}TPPDL showed no singlet oxygen production at all after irradiation by a 635 nm laser beam. Although the reasons for the unexpected behavior of *cis*-H_2F_{20}TPPDL, the results showed that the orientation of dilactone moieties affects the singlet oxygen production.

The photocytoxicity of *trans*- and *cis*-H_2F_{20}TPPDL and their zinc complexes in HeLa cells was investigated to explore their potential utility for use as photosensitizes in PDT. We used the modified solvent extraction/evaporation single-emulsion method[9] to prepare porphodilactones-loaded poly(lactide-*co*-glycolide) nanoparticles (PLGA NPs) to make the four porphodilactones water-soluble. MTT assays were carried out to investigate the dark toxicity and phototoxicity of the NPs in HeLa cells. Both compounds showed no dark toxicity after incubation for 24 h in HeLa cells (Figure 9). After irradiation with a 671 nm laser at a power of 20 mW cm^{-2} for 60 s, *trans*-H_2F_{20}TPPDL and its zinc complex-loaded PLGA NPs exhibited good phototoxicity with a half-maximal inhibitory concentration (IC_{50}) value of 51 and 44 $\mu g \cdot mL^{-1}$, respectively. However, the IC_{50} value of *cis*-ZnF_{20}TPPDL-loaded PLGA NPs was significantly larger (94 $\mu g \cdot mL^{-1}$), despite having a larger Φ_Δ value, which may be related to its low red light (671 nm) absorption ability. The Propidium iodide (PI) staining experiment (Figure 10) showed that most of the cells were dead after incubation with 60 $\mu g \cdot mL^{-1}$ *trans*-H_2F_{20}TPPDL and its zinc complex-loaded PLGA NPs for 24h and then irradiated by using a 671 nm laser at a power of 20 mW cm^{-2} for 60 s, while less cell death was observed for the *cis*-ZnF_{20}TPPDL-loaded PLGA NPs under identical condition. As expected, *cis*-H_2F_{20}TPPDL-loaded PLGA NPs showed nearly no photocytoxicity toward Hela cells, which was consistent with the zero singlet oxygen production and the MTT results.

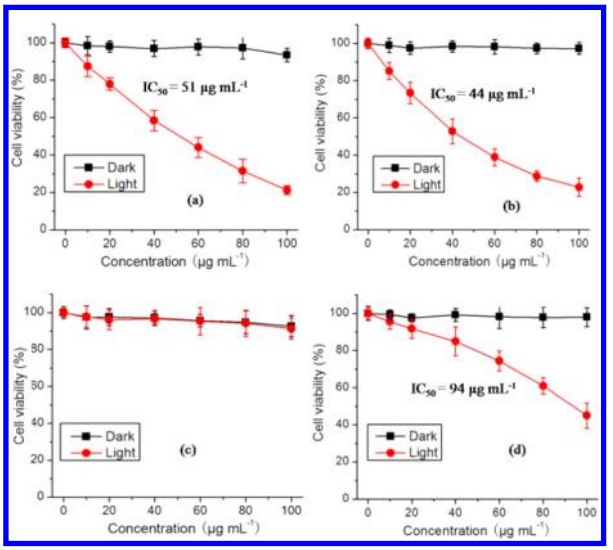

Figure 9. Dark toxicity and phototoxicity of (a) *trans*-H_2F_{20}TPPDL, (b) *trans*-ZnF_{20}TPPDL, (c) *cis*-H_2F_{20}TPPDL, (d) *cis*-ZnF_{20}TPPDL-loaded PLGA NPs in HeLa cells. Irradiated after a 671 nm laser at a power of 20 mW cm^{-2} for 60 s and then analyzed by MTT assay.

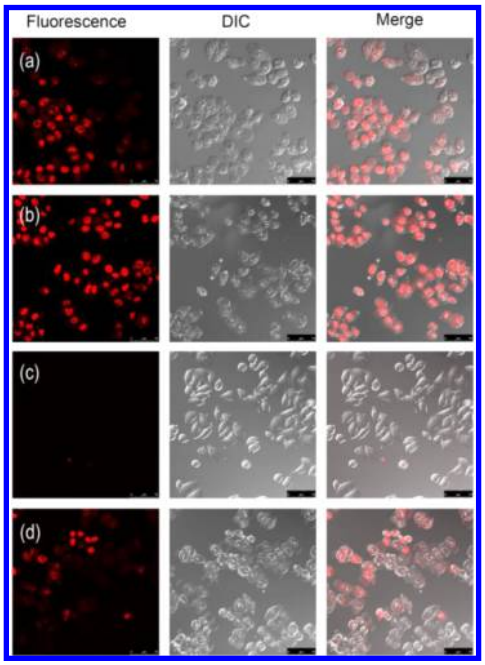

Figure 10. Confocal fluorescence images of PI stained HeLa cells treated with 60 $\mu g \cdot mL^{-1}$ (a) *trans*-H_2F_{20}TPPDL, (b) *trans*-H_2F_{20}TPPDL, (c) *cis*-H_2F_{20}TPPDL, (d) *cis*-ZnF_{20}TPPDL-loaded PLGA NPs incubation combined with irradiation. Scale bar: 75 μm (DIC: differential interference contrast).

CONCLUSIONS

The free base *cis* and *trans* opp-porphodilactone isomers and their zinc complexes have been successfully isolated and characterized. A detailed analysis of their optical spectra and TD-DFT calculations has demonstrated that the electronic structures are similar to those of bacteriochlorins. The relative orientation of the carbonyl bonds plays a significant role in determining the optical properties in the Q-band region, since it has a significant impact on the relative energies of the frontier π-MOs. Moreover, an investigation of the photophysical properties and in-depth photocytotoxicity studies has demon-

dx.doi.org/10.1021/ja502729x | J. Am. Chem. Soc. XXXX, XXX, XXX−XXX

strated the potential utility of these compounds as PDT photosensitizers for use in the biological window between 650 and 1000 nm. The novel strategy reported here should open the door to design of more novel NIR absorbing porphyrinoids.

EXPERIMENTAL SECTION

Unless otherwise stated, all reactions were performed under an inert nitrogen atmosphere. UV−vis spectra were recorded on an Agilent 8453 UV−vis spectrometer equipped with an Agilent 89090A thermostat (±0.1 °C) at 25.0 °C. The emission spectra and lifetimes were recorded on an Edinburgh Analytical Instruments FLS920 lifetime and steady state spectrometer (450 W Xe lamp, PMT R928). Mass spectra were measured on a Bruker APEX IV FT-ICR Mass Spectrometer (ESI-MS). IR spectra were recorded on a Bruker Vector22 FT-IR spectrometer as KBr pellets. ^{1}H NMR spectra were measured on a Bruker ARX400 (400 MHz) or AVANCE III (500 MHz) spectrophotometer; ^{19}FNMR (CF_3COOH as external standard) and ^{13}C NMR spectra were recorded on a Bruker AVANCE III spectrophotometer (471 MHz for ^{19}F, 126 MHz for ^{13}C). Spectroscopic-grade DCM was used as purchased from Alfa-Aesar, for the various optical measurements. MCD spectra were recorded on a Jasco J-725 spectrodichrometer with a Jasco electromagnet that produced a magnetic field of up to 1.09 T. $CHCl_3$ that was stabilized by 0.5% EtOH (Nacalai Tesque) was used as the solvent. The modified conventions of Piepho and Schatz[18] are adopted for the three Faraday terms, so in contrast with many earlier studies by authors such as Michl,[14] the sign of Faraday $\mathcal{B}_0$ terms matches that of the spectral measurements.

Synthesis of 5,10,15,20-Tetra(pentafluorophenyl)-porphodilactone (mixture of two isomers). *Method 1.* 5,10,15,20-tetra(pentafluorophenyl)porphyrin (0.1 mmol 100 mg) was dissolved in 1,2-dichloroethane (DCE) (45 mL). The DCE solution and 15 mL of water were mixed and stirred at room temperature, and an aqueous $RuCl_3$ solution (4.3 mg 0.02 mmol) and a DCE solution of 2,2′-bipyridine (3.2 mg, 0.02 mol) were added to the system. The solution was then heated to 70 °C, and a mixture of Oxone and NaOH solution (12 equiv) was added by dropping funnel. The reaction was monitored by TLC and quenched with an aqueous solution of $Na_2S_2O_3$. The organic phase was separated by separating funnels, the aqueous phase was washed twice with DCM, and the combined organic phase was evaporated by rotary evaporation. A mixture of two 5,10,15,20-tetra(pentafluorophenyl)porphodilactone isomers was obtained by column chromatography as a purple solid in the yield of 45%. The *trans*-H_2F_{20}TPPDL:*cis*-H_2F_{20}TPPDL ratio was determined to be 3:2 from the integration of the ^{1}H NMR data.

Method 2. 5,10,15,20-tetra(pentafluorophenyl)porpholactone, was used as the starting material, and the synthesis procedure was similar to Method 1, but the amount of oxidant (Oxone:NaOH = 1:1 solution) was (4 equiv). 5,10,15,20-tetra(pentafluorophenyl) porphodilactone was obtained in 53% yield as a mixture of two isomers.

Synthesis of *trans*- and *cis*-ZnF_{20}TPPDL. A 5,10,15,20-tetra-(pentafluorophenyl)porphodilactone (1.0 g, 1 mmol) and $Zn(AcO)_2\cdot 2H_2O$ (2.2 g, 10 mmol) mixture was dissolved in $CHCl_3$/MeOH (v/v = 7:3) and was refluxed for 4h. The product (mixture of two isomers) was isolated by column chromatography as a green solid in quantitative yield. In a typical isolation run, the zinc 5,10,15,20-tetrakispentafluorophenylporphodilactones (600 mg) were carefully separated by column chromatography using petroleum ether/ethyl acetate (v/v = 15:1) as the eluent. *trans*-ZnF_{20}TPPDL (110 mg) can be isolated from the first chromatography fraction, and *cis*-ZnF_{20}TPPDL (45 mg) can be accumulated by repeating the column chromatography process another two times. The separation process was monitored by UV−vis spectroscopy by monitoring differences in the $Q_{y(0,0)}$ bands. The purity of the product was checked by ^{1}H NMR spectroscopy. *trans*-ZnF_{20}TPPDL: ^{1}H NMR (400 MHz, $CDCl_3$) δ 8.70 (s, 4H). ^{13}C NMR (126 MHz, $CDCl_3$) δ 164.46, 159.99, 151.27, 150.41, 147.24, 145.24, 143.68, 141.68, 139.15, 137.14, 131.88, 131.34, 126.54, 111.92, 111.33, 104.18, 90.95. HRMS (ESI$^+$) m/z [M + H]$^+$: calcd for $C_{42}H_5F_{20}N_4O_4Zn$ 1072.9283, found: 1072.9248; *cis*-ZnF_{20}TPPDL: ^{1}H NMR (400 MHz, $CDCl_3$) δ 8.57 (s, 2H), 8.43 (s, 2H). ^{13}C NMR (126 MHz, $CDCl_3$) δ 164.38, 155.58, 153.15, 148.33, 147.96, 146.87, 145.82, 145.16, 143.69, 141.65, 139.17, 137.15, 133.69, 133.07, 129.16, 123.44, 111.92, 110.96, 109.01, 88.72. HRMS (ESI$^+$) m/z [M + H]$^+$: calcd for $C_{42}H_5F_{20}N_4O_4Zn$ 1072.9283, found: 1072.9275.

Synthesis of *trans*-H_2F_{20}TPPDL. Concentrated HCl solution (36−38%) (0.3 mL) were added to 5 mL acetone solution of *trans*-ZnF_{20}TPPDL (100 mg, 0.09 mmol) at room temperature, and after several minutes the color of the solution changed from green to purple. *trans*-H_2F_{20}TPPDL was obtained in quantitative yield. ^{1}H NMR (500 MHz, $CDCl_3$) δ 8.86 (d, J = 1.7 Hz, 4H), −2.12 (s, 2H). ^{13}C NMR (126 MHz, $CDCl_3$) δ 165.09, 153.70, 147.27, 145.32, 144.02, 142.00, 139.31, 138.84, 137.29, 133.10, 128.21, 127.91, 110.77, 103.42, 91.80. HRMS (ESI$^+$) m/z [M + H]$^+$: calcd for $C_{42}H_7F_{20}N_4O_4$ 1011.0148, found: 1011.0139.

Synthesis of *cis*-H_2F_{20}TPPDL. was obtained through a process similar to that described for *trans*-H_2F_{20}TPPDL. ^{1}H NMR (500 MHz, $CDCl_3$) δ 8.70 (d, J = 1.4 Hz, 2H), 8.53 (d, J = 2.0 Hz, 2H), −0.32 (s, 1H), −0.94 (s, 1H). ^{13}C NMR (126 MHz, $CDCl_3$) δ 165.06, 155.95, 147.12, 145.29, 144.06, 142.76, 141.87, 139.27, 137.38, 136.58, 130.27, 130.20, 125.63, 110.77, 109.89, 107.94, 90.41. HRMS (ESI$^+$) m/z [M + H]$^+$ calcd for $C_{42}H_7F_{20}N_4O_4$ 1011.0148, found: 1011.0173.

Singlet Oxygen Quantum Yield Determination. Singlet oxygen quantum yields (Φ_Δ) of H_2F_{20}TPP, H_2F_{20}TPPL, *trans*- and *cis*-H_2F_{20}TPPDLs and their zinc complexes were calculated using DPBF as a singlet oxygen scavenger[19] with MB as standard (Φ_Δ = 0.57 in DCM).[20] The Φ_Δ values were calculated according to the following equation:

$$\Phi_\Delta(^1O_2)^{por} = \Phi_\Delta(^1O_2)^{MB}\frac{S^{por}F^{MB}}{S^{MB}F^{por}}$$

Where $\Phi_\Delta(^1O_2)$ is the quantum yield of singlet oxygen, superscripts por and MB represent mentioned porphyrinoids and methylene blue, respectively. S is the slope of a plot of difference in change in absorbance of DPBF (at 411 nm) with the irradiation time, and F is the absorption correction factor, which is given by $F = 1-10^{-OD}$ (OD at the irradiation wavelength).

Synthesis of Porphodilactones Loaded PLGA-NPs. The *trans*- and *cis*-H_2F_{20}TPPDLs and their zinc complexes loaded PLGA NPs were prepared using a modified solvent extraction/evaporation single-emulsion method.[9] 10 mg of poly(lactide-*co*-glycolide) (PLGA, Daigang Biomaterial Co., Ltd., Jinan, China) and 5 μmol *trans*-H_2F_{20}TPPDL, *trans*-ZnF_{20}TPPDL, *cis*-H_2F_{20}TPPDL or *cis*-ZnF_{20}TPPDL were dissolved into 1 mL DCM. The organic solution was added dropwise to 10 mL of aqueous solution rotating at 5000 rpm containing poly(vinyl alcohol) (PVA, 2.5 wt % in ultrapure water; M_W = 30,000−70,000 Da from Sigma−Aldrich) as a surfactant, sonicated for 2 min at 4 °C and then stirred overnight to evaporate the organic solvent, forming porphyrin-loaded PLGA NPs. After removing large particles by centrifugation at 3000 g for 25 min, the PLGA NPs were collected by ultracentrifugation at 21,000 g for 25 min and washed three times to remove excess PVA. In between the washing steps, PLGA NPs were redispersed into ultrapure water by sonication. The washed PLGA NPs were filtered with a 0.45 μm membrane filter and stored at 4 °C until use.

MTT Assay. (3-(4,5-Dimethylthiazol-2-yl)-2,5-diphenyl tetrazolium bromide) (MTT) assay was carried out to investigate the dark toxicity and phototoxicity of the *trans*- and *cis*-H_2F_{20}TPPDLs and their zinc complexes loaded PLGA NPs. HeLa cells were first seeded in two 96-well plates at a seeding density of 1×10^4 cells per well in 200 μL complete medium, which was incubated at 37 °C for 24 h. After rinsing with PBS, HeLa cells were incubated with 200 μL culture media containing serial concentrations of porphodilactone loaded PLGA NPs for 24 h. One plate was kept in the dark to study the dark toxicity, and another plate was irradiated using a 671 nm laser at a power of 20 mW cm^{-2} for 60 s. Afterward, the cells were grown for another 24 h. Then, 20 μL of 5 mg mL^{-1} MTT solution in pH 7.4 PBS was added to each well. After 4h incubation, the medium containing

dx.doi.org/10.1021/ja502729x | J. Am. Chem. Soc. XXXX, XXX, XXX−XXX

unreacted MTT was carefully removed, and 200 μL of DMSO was added to each well to dissolve any blue formazan that had been produced. After 1 h the optical density (OD) at a wavelength of 490 nm was measured with a Bio-Rad microplate reader. The cell viability was determined by the following equation: Cell viability (%) = (mean of OD value of treatment group/mean OD value of control) × 100%.

Confocal Imaging (PI Staining). HeLa cells were seeded in 35 mm confocal dishes (Glass Bottom Dish) at a density of 1×10^4 per dish and incubated in complete medium for 24 h at 37 °C. The medium was then replaced with fresh culture medium containing 60 μg mL^{-1} porphodilactone loaded PLGA NPs to incubate for 24 h at 37 °C. The cells were irradiated with a 671 nm laser at a power of 20 mW cm^{-2} for 60 s and were then stained with 2 μM PI for 15 min so that cell death can be visualized by confocal laser scanning microscope (CLSM; TCS SP5, Leica, Germany). The PI solution was excited at 543 nm with an argon ion laser, and the emission was collected from 600 to 630 nm.

Theoretical Calculations. The density functional theory (DFT) method was used to carry out geometry optimizations for porphodilactones by using the B3LYP functional with 6-31G(d) basis sets. The CAM-B3LYP functional was used with 6-31G(d) basis sets to calculate the UV−vis absorption properties based on the time-dependent (TD-DFT) method. The calculations were performed with the Gaussian09 program package.

■ ASSOCIATED CONTENT

Ⓢ Supporting Information

Detailed isolation, photophysical and crystallographic data; ^1H, ^{13}C NMR and ^{19}F NMR, UV−vis absorption, IR, and ESI-MS spectra; the details of the TD-DFT calculations; and complete ref 11. These materials are available free of charge via the Internet at http://pubs.acs.org.

■ AUTHOR INFORMATION

Corresponding Authors

zhangjunlong@pku.edu.cn
zshen@nju.edu.cn

Notes

The authors declare no competing financial interest.

■ ACKNOWLEDGMENTS

Support from the National Key Basic Research Support Foundation of China (NKBRSFC) (2010CB912302), NSFC (grant no. 20971007, 21271013 to J.L.Z. and 21371090 to Z.S.) and the National Fund for Fostering Talents of Basic Sciences (J1030413) to J.Z.C. is gratefully acknowledged. Theoretical calculations were carried out at the Centre for High Performance Computing in Cape Town.

■ REFERENCES

(1) (a) *Advances in Photosynthesis and Respiration*; Grimm, B., Porra, R., Rüdiger, W., Scheer, H., Eds.; Springer: Dordrecht, 2006; Vol. 25: Chlorophylls and Bacteriochlorophylls. (b) Rüdiger, W. In *Advances in Photosynthesis and Respiration*; Grimm, B., Porra, R., Rüdiger, W., Scheer, H., Eds.; Springer: Dordrecht, 2006; Vol. 25: Chlorophylls and Bacteriochlorophylls, pp 189−200. (c) Larkum, A. W. D. In *Advances in Photosynthesis and Respiration*; Grimm, B., Porra, R., Rüdiger, W., Scheer, H., Eds.; Springer: Dordrecht, 2006; Vol. 25: Chlorophylls and Bacteriochlorophylls, pp 261−282. (d) Scheer, H. In *Advances in Photosynthesis and Respiration*; Grimm, B., Porra, R., Rüdiger, W., Scheer, H., Eds.; Springer: Dordrecht, 2006; Vol. 25: Chlorophylls and Bacteriochlorophylls, pp 1−26. (e) Kräutler, B. *Angew. Chem., Int. Ed.* **2011**, *50*, 2439.

(2) (a) Neves, M.; Martins, R. M.; Tome, A. C.; Silvestre, A. J. D.; Silva, A. M. S.; Felix, V.; Drew, M. G. B.; Cavaleiro, J. A. S. *Chem. Commun.* **1999**, 385. (b) Kobayashi, N.; Nakajima, S.; Ogata, H.; Fukuda, T. *Chem.—Eur. J.* **2004**, *10*, 6294. (c) Sankar, J.; Mori, S.; Saito, S.; Rath, H.; Suzuki, M.; Inokuma, Y.; Shinokubo, H.; Suk Kim, K.; Yoon, Z. S.; Shin, J.-Y.; Lim, J. M.; Matsuzaki, Y.; Matsushita, O.; Muranaka, A.; Kobayashi, N.; Kim, D.; Osuka, A. *J. Am. Chem. Soc.* **2008**, *130*, 13568. (d) Wu, D.; Descalzo, A. B.; Weik, F.; Emmerling, F.; Shen, Z.; You, X. Z.; Rurack, K. *Angew. Chem., Int. Ed.* **2008**, *47*, 193. (e) Toganoh, M.; Furuta, H. *Chem. Commun.* **2012**, *48*, 937. (f) Matsushita, O.; Derkacheva, V. M.; Muranaka, A.; Shimizu, S.; Uchiyama, M.; Luk'yanets, E. A.; Kobayashi, N. *J. Am. Chem. Soc.* **2012**, *134*, 3411.

(3) Chen, M.; Schliep, M.; Willows, R. D.; Cai, Z.-L.; Neilan, B. A.; Scheer, H. *Science* **2010**, *329*, 1318.

(4) (a) Crossley, M. J.; King, L. G. *J. Chem. Soc., Chem. Commun.* **1984**, 920. (b) Gouterman, M.; Hall, R. J.; Khalil, G. E.; Martin, P. C.; Shankland, E. G.; Cerny, R. L. *J. Am. Chem. Soc.* **1989**, *111*, 3702. (c) McCarthy, J. R.; Jenkins, H. A.; Brückner, C. *Org. Lett.* **2003**, *5*, 19. (d) Brückner, C.; Ogikubo, J.; McCarthy, J. R.; Akhigbe, J.; Hyland, M. A.; Daddario, P.; Worlinsky, J. L.; Zeller, M.; Engle, J. T.; Ziegler, C. J.; Ranaghan, M. J.; Sandberg, M. N.; Birge, R. R. *J. Org. Chem.* **2012**, *77*, 6480. (e) Lv, H. B.; Yang, B. Y.; Jing, J.; Yu, Y.; Zhang, J.; Zhang, J. L. *Dalton Trans.* **2012**, *41*, 3116. (f) Yu, Y.; Lv, H. B.; Ke, X. S.; Yang, B. Y.; Zhang, J. L. *Adv. Syn. Catal.* **2012**, *354*, 3509.

(5) (a) Zelelow, B.; Khalil, G. E.; Phelan, G.; Carlson, B.; Gouterman, M.; Callis, J. B.; Dalton, L. R. *Sens. Actuators, B.* **2003**, *96*, 304. (b) Khalil, G. E.; Costin, C.; Crafton, J.; Jones, G.; Grenoble, S.; Gouterman, M.; Callis, J. B.; Dalton, L. R. *Sens. Actuators, B.* **2004**, *97*, 13. (c) Gouterman, M.; Callis, J.; Dalton, L.; Khalil, G.; Mebarki, Y.; Cooper, K. R.; Grenier, M. *Meas. Sci. Technol.* **2004**, *15*, 1986. (d) Waskitoaji, W.; Hyakutake, T.; Kato, J.; Watanabe, M.; Nishide, H. *Chem. Lett.* **2009**, *38*, 1164. (e) Waskitoaji, W.; Hyakutake, T.; Watanabe, M.; Nishide, H. *React. Funct. Polym.* **2010**, *70*, 669. (f) Khalil, G. E.; Daddario, P.; Lau, K. S. F.; Imtiaz, S.; King, M.; Gouterman, M.; Sidelev, A.; Puran, N.; Ghandehari, M.; Brückner, C. *Analyst* **2010**, *135*, 2125. (g) Yu, Y.; Czepukojc, B.; Jacob, C.; Jiang, Y.; Zeller, M.; Brückner, C.; Zhang, J.-L. *Org. Biomol. Chem.* **2013**, *11*, 4613. (h) Tang, J.; Chen, J.-J.; Jing, J.; Chen, J.-Z.; Lv, H.; Yu, Y.; Xu, P.; Zhang, J.-L. *Chem. Sci.* **2014**, *5*, 558.

(6) Gouterman, M. *The Porphyrins*; Dolphin, D., Ed.; Academic Press: New York, 1978; Vol. 3, Part A, pp 1−165.

(7) Ethirajan, M.; Chen, Y. H.; Joshi, P.; Pandey, R. K. *Chem. Soc. Rev.* **2011**, *40*, 340.

(8) Cakmak, Y.; Kolemen, S.; Duman, S.; Dede, Y.; Dolen, Y.; Kilic, B.; Kostereli, Z.; Yildirim, L. T.; Dogan, A. L.; Guc, D.; Akkaya, E. U. *Angew. Chem., Int. Ed.* **2011**, *50*, 11937.

(9) (a) Li, K.; Pan, J.; Feng, S.-S.; Wu, A. W.; Pu, K.-Y.; Liu, Y.; Liu, B. *Adv. Funct. Mater.* **2009**, *19*, 3535. (b) Zhang, Z. P.; Tongchusak, S.; Mizukami, Y.; Kang, Y. J.; Ioji, T.; Touma, M.; Reinhold, B.; Keskin, D. B.; Reinherz, E. L.; Sasada, T. *Biomaterials* **2011**, *32*, 3666.

(10) (a) Mack, J.; Stillman, M. J.; Kobayashi, N. *Coord. Chem. Rev.* **2007**, *251*, 429. (b) Kobayashi, N.; Muranaka, A.; Mack, J. *Circular Dichroism and Magnetic Circular Dichroism Spectroscopy for Organic Chemists*; Royal Society of Chemistry: London, 2011.

(11) Frisch, M. J., et al. *Gaussian 09*, revision A.02; Gaussian, Inc., Wallingford, CT, 2009. Complete reference is in Supporting Information.

(12) Cai, Z.-L.; Crossley, M. J.; Reimers, J. R.; Kobayashi, R.; Amos, R. D. *J. Phys. Chem. B* **2006**, *110*, 15624.

(13) (a) Moffitt, W. *J. Chem. Phys.* **1954**, *22*, 320. (b) Moffitt, W. *J. Chem. Phys.* **1954**, *22*, 1820.

(14) (a) Michl, J. *J. Am. Chem. Soc.* **1978**, *100*, 6801. (b) Michl, J. *Pure Appl. Chem.* **1980**, *52*, 1549. (c) Michl, J. *Tetrahedron* **1984**, *40*, 3845.

(15) (a) Mack, J.; Stillman, M. J. *Porphyrin Handbook*; Kadish, K. M., Smith, K. M., Guilard, R., Eds.; Academic Press: New York, 2003; Vol. 16, Ch. 103, pp 43−116. (b) Mack, J.; Stillman, M. J. *Coord. Chem. Rev.* **2001**, *219*, 993.

(16) Perrin, M. H. *J. Chem. Phys.* **1973**, *59*, 2090.

(17) (a) Keegan, J. D.; Stolzenberg, A. M.; Lu, Y. C.; Linder, R. E.; Barth, G.; Moscowitz, A.; Bunnenberg, E.; Djerassi, C. *J. Am. Chem.*

Soc. **1982**, *104*, 4317. (b) Keegan, J. D.; Stolzenberg, A. M.; Lu, Y. C.; Linder, R. E.; Barth, G.; Moscowitz, A.; Bunnenberg, E.; Djerassi, C. *J. Am. Chem. Soc.* **1982**, *104*, 4305. (c) Djerassi, C.; Lu, Y.; Waleh, A.; Shu, A. Y. L.; Goldbeck, R. A.; Kehres, L. A.; Crandell, C. W.; Wee, A. G. H.; Knierzinger, A.; Gaeteholmes, R.; Loew, G. H.; Clezy, P. S.; Bunnenberg, E. *J. Am. Chem. Soc.* **1984**, *106*, 4241.

(18) Piepho, S. B.; Schatz, P. N. In *Group Theory in Spectroscopy with Applications to Magnetic Circular Dichroism*; Wiley: New York, 1983.

(19) (a) Morone, M.; Beverina, L.; Abbotto, A.; Silvestri, F.; Collini, E.; Ferrante, C.; Bozio, R.; Pagani, G. A. *Org. Lett.* **2006**, *8*, 2719. (b) Rossi, L. M.; Silva, P. R.; Vono, L. L. R.; Fernandes, A. U.; Tada, D. B.; Baptista, M. c. S. *Langmuir* **2008**, *24*, 12534.

(20) (a) Mirenda, M.; Strassert, C. A.; Dicelio, L. E.; Roman, E. S. *ACS Appl. Mater. Interfaces* **2010**, *2*, 1556. (b) Thomas, A. P.; Saneesh Babu, P. S.; Asha Nair, S.; Ramakrishnan, S.; Ramaiah, D.; Chandrashekar, T. K.; Srinivasan, A.; Radhakrishna Pillai, M. *J. Med. Chem.* **2012**, *55*, 5110.